A correction method for the telluric absorptions and application to Lijiang Observatory

Kai-Xing Lu[1,2], Zhi-Xiang Zhang[3], Ying-Ke Huang[4], An-Bing Ren[5], Liang Xu[1,2], Hai-Cheng Feng[1,2], Yu-Xin Xin[1,2], Xu Ding[1,2], Xiao-Guang Yu[1,2] and Jin-Ming Bai[1,2]

[1] Yunnan Observatories, Chinese Academy of Sciences, Kunming 650011, China; *lukx@ynao.ac.cn*
[2] Key Laboratory for the Structure and Evolution of Celestial Objects, Chinese Academy of Sciences, Kunming 650011, China
[3] Department of Astronomy, Xiamen University, Xiamen 361005, China; *zhangzx@xmu.edu.cn*
[4] Qian Xuesen Laboratory of Space Technology, China Academy of Space Technology, Beijing 100094, China
[5] Department of Astronomy, China West Normal University, Nanchong 637002, China

Abstract Observing a telluric standard star for correcting the telluric absorption lines of spectrum will take a significant amount of precious telescope time, especially in the long-term spectral monitoring project. Beyond that, it is difficult to select a suitable telluric standard star near in both time and airmass to the scientific object. In this paper, we present a method of correcting the telluric absorption lines by combining the advantages of long slit spectroscopy. By rotating the slit, we observed the scientific object and a nearby comparison star in one exposure, so that the spectra of both objects should have the same telluric transmission spectrum. The telluric transmission spectrum was constructed by dividing the observed spectrum of the comparison star by its stellar template, and was used to correct the telluric absorption lines of the scientific object. Using the long slit spectrograph of the Lijiang 2.4-meter telescope, we designed a long-term spectroscopic observation strategy, and finished a four-year spectroscopic monitoring for a pair of objects (an active galactic nucleus and a non-varying comparison star). We applied this method to correct the telluric absorption lines of the long-term monitored spectra by the Lijiang 2.4-meter telescope, and investigated the variation of the telluric absorptions at Lijiang Observatory. We found that the telluric absorption transparency is mainly modulated by the seasonal variability of the relative humidity, airmass and seeing. Using the scatter of the [O III] $\lambda 5007$ fluxes emitted from the narrow-line region of active galactic nuclei as an indicator, we found that the correction accuracy of the telluric absorption lines is 1%.

Key words: techniques: telluric absorption — methods: data analysis — techniques: spectroscopic — quasars: individual (SDSS J1536+0441)

1 INTRODUCTION

Ground-based optical and near-infrared spectra are contaminated by the variable absorptions of the telluric atmosphere. In order to retrieve the intrinsic spectral signal of a scientific object, the traditional method is to observe a telluric standard star (early-type star) near in both time and airmass to the scientific object, then using the telluric spectrum created from standard star to correct the telluric absorption features by dividing the object's spectrum during the data reduction. Often, a rapidly rotating hot star (spectral type A or late B) is frequently adopted as the telluric standard because there are few and weak metal lines in the spectrum around the telluric absorption bands.

In addition, many sophisticated methods have been developed. For example, using G2 V star as telluric standards and the high-resolution spectrum of the Sun, Maiolino et al. (1996) developed a correction method for the telluric absorption lines. Combining Maiolino et al. (1996)'s method with above traditional early-type star method, Hanson et al. (1996, 2005) developed a method to correct the telluric absorption lines, which has to observe an A-star and a G2 V star and involves a somewhat tedious and complicated reduction process. Vacca et al. (2003) described a new method of generating a telluric correction spectrum by using observations of A0 V stars and a high-resolution model spectrum of Vega, which is similar to the process described by Maiolino et al. (1996).

Another approach is to generate a theoretical telluric absorption spectrum of the atmospheric transmission from a line database and the observing condition. Based on the available radiative transfer model, this approach has been successfully developed by several groups (e.g., Seifahrt et al. 2010; Gullikson et al. 2014; Bertaux et al. 2014; Cotton et al. 2014). Furthermore, some groups incorporated the radiative transfer model into their own code to fit an entire input spectrum (e.g., Husser et al. 2013; Gullikson et al. 2014; Smette et al. 2015).

Actually, the above methods have several disadvantages (e.g., Seifahrt et al. 2010; Gullikson et al. 2014): (1) It is difficult to find a suitable telluric standard star near in both time and airmass to the scientific object during the observation. (2) The strength of telluric absorption lines may significantly changes with the varying observing conditions (such as the weather, airmass and seeing), even if we find an ideal telluric standard star; it is almost impossible to obtain the spectrum of scientific object and telluric standard star under the same observing conditions. (3) If we conduct a long-term spectral monitoring study, observing a telluric standard star near the same time to the object, we will take a significant amount of precious telescope time. (4) The deviation of the modelled telluric absorption spectrum is mainly due to the limited accuracy of the meteorological data and errors in the radiative transfer model. Therefore, in this paper, we described a new method of correcting the telluric absorption lines from the spectrum, and used it to investigate the variation of telluric absorptions of Lijiang Observatory.

The paper is organised as follows. In Section 2, we described the correction method for the telluric absorption lines of spectrum. We applied this method to the spectra observed by the Lijiang 2.4-meter telescope in Section 3, including observation, data reduction, the telluric absorption correction, accuracy evaluation, and investigated the telluric absorption features of Lijiang Observatory. Sections 4 and 5 are discussion and summary, respectively.

2 METHOD

2.1 Long Slit Spectroscopy

The spectrograph used in astronomy is often equipped with a long slit (with different projected slit width), so that we can orient the long slit to take the spectra of the scientific object and a nearby non-varying comparison star simultaneously. This observation method is widely used in the reverberation mapping of active galactic nuclei to measure supermassive black hole mass and investigate the physics of the broad-line region (e.g., Maoz et al. 1990; Kaspi et al. 2000; Lu et al. 2019), because the spectrum of the non-varying comparison star can be used as the fiducial spectrum to calibrate the flux of

Table 1 Telluric absorption bands and selected windows in the optical region. "B∗" means the number of the telluric absorption bands (Col. (1)), these absorption bands with different absorption widths (Col. (3)) are caused by different absorbers (Col. (2)).

No (1)	Molecular (2)	Windows (3)
B1	O_2 (γ band)	6270 Å∼6350 Å
B2	O_2 (B band) + H_2O	6830 Å∼7050 Å
B3	H_2O	7143 Å∼7369 Å
B4	O_2 (A band)	7550 Å∼7750 Å
B5	H_2O	8080 Å∼8380 Å
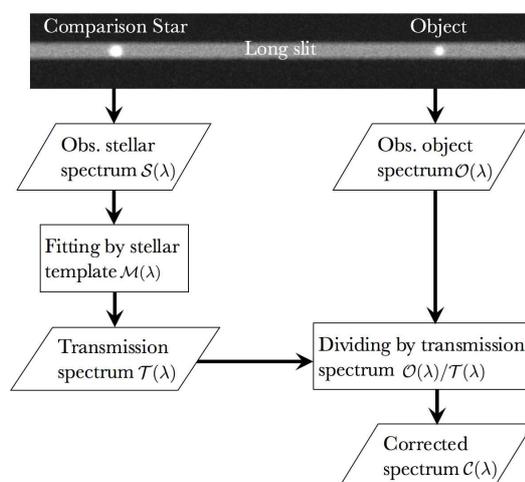
Fig. 1 Schematic diagram of correction for the telluric absorption lines.

scientific object in high precision (e.g., see Lu et al. 2019). The second application of the comparison star spectrum is to correct the line broadening caused by seeing and instruments (Du et al. 2016). In the application of correcting instrument broadening, the line broadening function can be obtained from the fitting between the comparison star spectrum and its stellar template, then we use the broadening function to correct the broadening of the emission-line profile through Richardson−Lucy deconvolution algorithm (Richardson 1972; Lucy 1974). Here we provide a new application of the comparison star spectrum.

2.2 Fitting Spectrum and Correcting Telluric Absorptions

In the scheme of long slit spectroscopy, the spectra of the scientific object and comparison star are obtained simultaneously. Extraction processes of the observed object and stellar spectra are similar to the works of Lu et al. (2016b) and Lu et al. (2019) (more details refer to Sect. 3). The schematic diagram of correcting the telluric absorption lines is shown in Figure 1. We first obtain
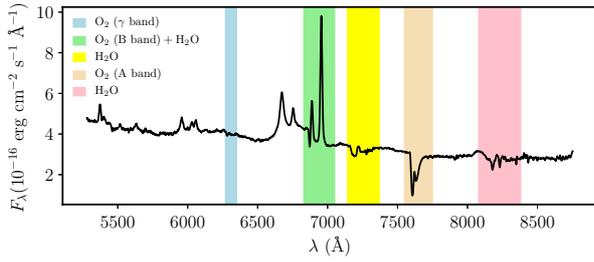
Fig. 2 The spectrum of SDSS J153636.22+044127.0 (J1536) observed by the Lijiang 2.4-meter telescope. Five telluric absorption bands in the observed spectrum are marked by colour diagram (see Table 1).

Fig. 3 The top panel is an example of fitting observed spectrum $\mathcal{C}(\lambda)$ by the stellar template, the observed spectrum of comparison star in *blue*, and scaled stellar template $\mathcal{C}'(\lambda)$ in *red*. The bottom panel is the residual of fitting regions.

the telluric transmission spectrum by fitting the spectrum of comparison star by a stellar template. Generally, there are two approaches to select the stellar template of the comparison star: (1) selecting the most similar stellar spectrum from the library of synthesis stellar model as the template of the comparison star (e.g., Husser et al. 2013); (2) searching the calibrated spectra of the comparison star from spectral survey database (e.g., SDSS, LAMOST) as the template of the comparison star[1]. To fit the observed spectrum of the comparison star, the selected stellar template $\mathcal{M}(\lambda)$ is shifted, broadened and scaled. That is the observed spectrum $\mathcal{S}(\lambda)$ of the comparison star is modelled by function

$$\mathcal{S}'(\lambda) = \mathcal{P}(\lambda)[\mathcal{M}(\lambda) \otimes \mathcal{G}(\text{Shift, FWHM})]. \quad (1)$$

Here, $\mathcal{P}$ is a Legendre polynomial that accounts for the mismatch in the continuum shape of comparison star and stellar template, and $\mathcal{G}$ is a Gaussian kernel with parameters of velocity and shift that accounts for the mismatch in the line width and shift of the intrinsic absorption lines.

It should be noted that the telluric absorptions from the red side of the optical spectrum to the near infrared are mainly caused by O_2 and H_2O. The main telluric absorption bands include narrow oxygen bands (identified as the Fraunhofer γ, B, and A bands) and some comparably weak water vapour features. The telluric absorption bands of the optical region with bandwidths (i.e., absorption windows) are presented in Table 1 (see also Smette et al. 2015). During the fitting of the observed spectrum, the spectral region within the telluric absorption windows (see Table 1) are masked. Then the telluric transmission spectrum $\mathcal{T}(\lambda)$ in the selected absorption windows is constructed by dividing the observed spectrum of the comparison star $\mathcal{S}(\lambda)$ by the modelled spectrum $\mathcal{S}'(\lambda)$. Lastly, we obtained the telluric absorption corrected spectrum by dividing the observed object spectrum $\mathcal{O}(\lambda)$ by the telluric transmission spectrum $\mathcal{T}(\lambda)$, because the spectra of comparison star and the scientific object are
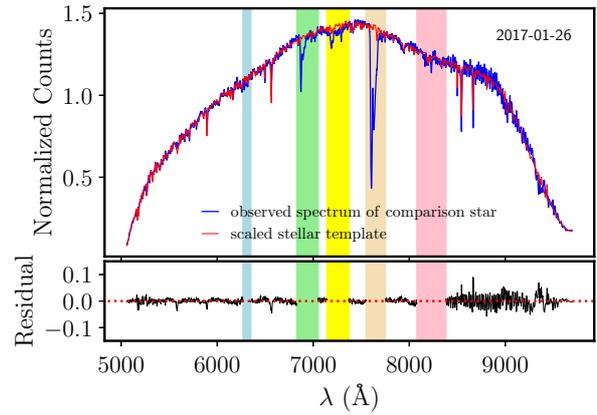
obtained at the same time and with the same airmass and seeing. In fact, this step resembles the process of `IRAF` telluric. Next, we use this method to correct the telluric absorption lines of the spectra observed by the Lijiang 2.4-meter telescope and investigate the variation of the telluric absorptions at Lijiang Observatory.

3 APPLICATION

The Lijiang 2.4-meter Telescope (LJT) is located at Lijiang Observatory (E: $100°01'48''$, N: $26°41'42''$, altitude: 3193 meters), and is administered by Yunnan Observatories of the Chinese Academy of Sciences. LJT observation time is opening to the worldwide astronomical community since 2008. The structure of the 2.4-meter telescope including optical, mechanical, motion and control systems along with its instruments are described by Fan et al. (2015) and Wang et al. (2019). Basic observing conditions (including seeing, wind speed, weather and so on) are presented in the recent paper of Xin et al. (2020). The Yunnan Faint Object Spectrograph and Camera (YFOSC) mounted on the 2.4-meter telescope is a versatile instrument for spectroscopy and photometry. As a versatile instrument, YFOSC is equipped with a series of Grisms, long slits and filters. The wavelength coverage of these Grisms is about 3600 Å∼9000 Å, the red side of spectrum observed by YFOSC is covered by some telluric absorption bands. Correction of the telluric absorption lines is an essential step to extract the spectral signals.

3.1 Observation Strategy and Spectral Monitoring

To estimate the correction accuracy of the telluric absorption lines using the above described method, and to investigate the variation of the telluric absorptions at

---

[1] *https://github.com/BU-hammerTeam/PyHammer*
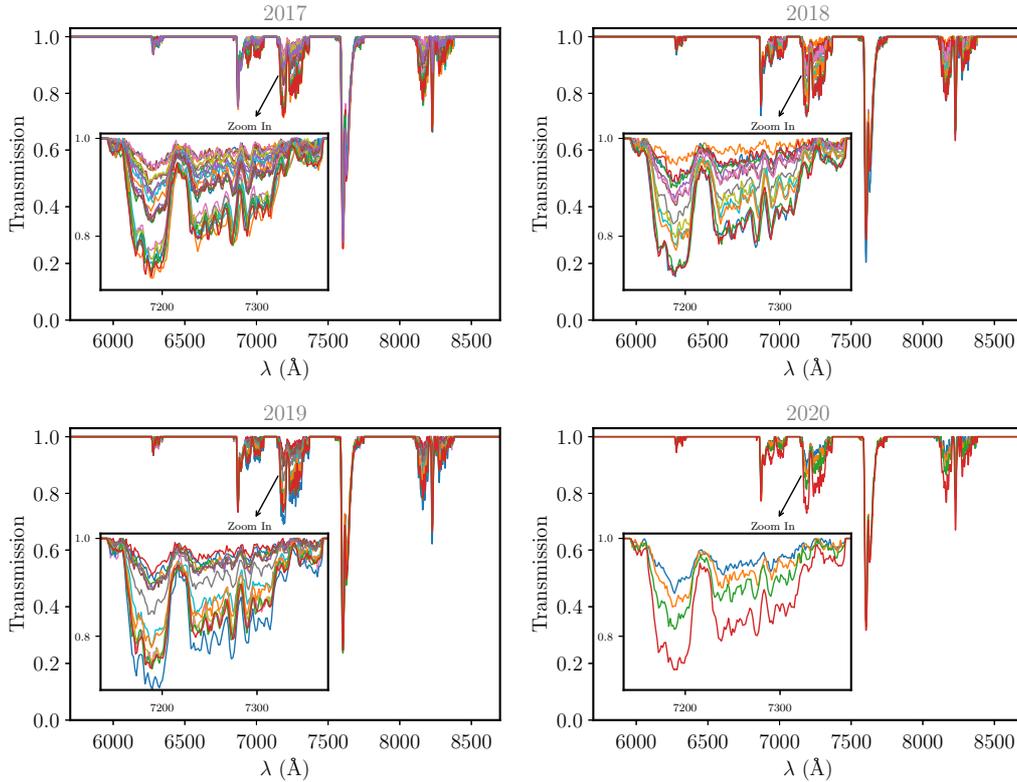
Fig. 4 The transmission spectra of Lijiang Observatory obtained in Sect. 3.3 provide values from 0 (totally opaque) to 1 (fully transparency). The year of observation was noted in the title of the panel, a transmission spectrum corresponds to one observation.

Lijiang observatory, we designed a strategy of long slit spectroscopy and developed a long-term spectroscopic monitoring project using the Lijiang 2.4-meter telescope. In the observation of active galactic nuclei, it is generally believed that the fluxes of the forbidden line [O III] $\lambda5007$ emitted from the narrow-line region are stable in the timescale of years (e.g., Foltz et al. 1981; Lu et al. 2016b, 2019). If the wavelength of [O III] $\lambda5007$ emission line locate in the telluric absorption band in the observed frame, the apparent variation of the [O III] $\lambda5007$ fluxes will be an indicator of the telluric absorptions and the scatter of [O III] $\lambda5007$ fluxes after correcting the telluric absorptions can also be used to estimate the correction accuracy. Therefore, we orient the long slit to take the spectra of the object SDSS J153636.22+044127.0 (J1536) and a non-varying comparison star simultaneously, where J1536 is an active galactic nucleus (AGN) with redshift 0.3889, and its optical spectrum observed by the Lijiang 2.4-meter telescope is shown in Figure 2. There are five telluric absorption bands in the observed spectra, which are listed in Table 1 and marked in Figure 2. In the observed frame, the [O III] $\lambda5007$ emission line of J1536 is in the B2 absorption band (see Fig. 2 and Table 1), we can measure the scatter of the [O III] $\lambda5007$ fluxes before and after correcting the telluric absorption lines and use to estimate the correction accuracy of the

telluric absorption lines. On the other hand, J1536 is a candidate of supermassive black hole binary (SMBHB, e.g., Boroson & Lauer 2009; Lu et al. 2016a; Zhang et al. 2019), except for investigating the variation of the telluric absorptions, we will use these long-term monitored spectra to investigate the broad-line region and optical variability physics of SMBHB. The latter will be presented in a separation paper.

We have finished a four-year spectroscopic monitoring for a pair of objects (J1536 *vs.* its comparison star). The observation started from 2017 and continued to 2020, and the annual spectral sampling lasts from January to September. All spectra of J1536 and comparison star are observed using Grism 8 mounted on the terminal of YFOSC, which provides a resolution of 78 Å mm^{-1} (1.5 Å pixel^{-1}) and covers the wavelength range 5000 Å∼9000 Å, which fully guaranteed the study of long-term variation of the telluric absorptions at Lijiang Observatory.

3.2 Data Reduction

Following the standard process included bias subtraction, flat-field correction, wavelength calibration and spectrum extraction, we reduced the two-dimensional spectroscopic data using the standard `IRAF(v2.16)` package. All
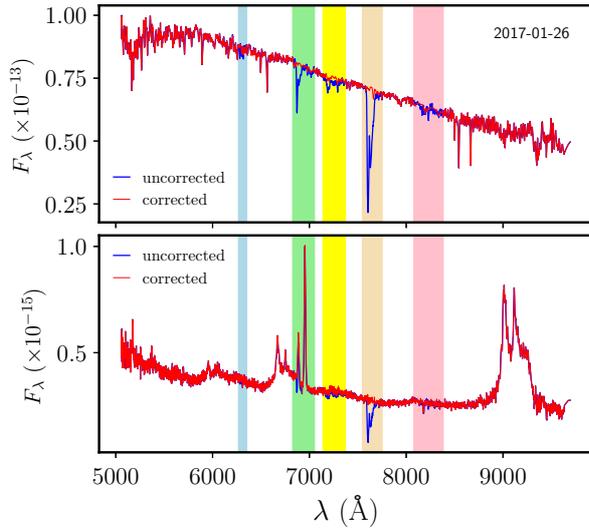
Fig. 5 Comparison of the telluric absorption corrected spectra (see Sect. 3.3) and uncorrected spectra in the observed frame. Only flux calibrated spectra are shown in *blue*, the telluric absorption corrected and flux calibrated spectra are shown in *red*. The units of F_λ is erg s^{-1} cm^{-2} Å^{-1}. The top panel shows the spectra of comparison star, and the bottom panel shows the spectra of J1536.

spectra were extracted using a uniform aperture of 20 pixels (5.7''), and background was determined from two adjacent regions ($+7.4'' \sim +14''$ and $-7.4'' \sim -14''$) on both sides of the aperture region. Spectral fluxes of the scientific object were calibrated by the comparison stars in two steps. (1) We produced a fiducial spectrum of the comparison star using the data from nights with photometric conditions. (2) For each object/comparison star pair, we obtained a wavelength-dependent sensitivity function by comparing the star's spectrum to the fiducial spectrum. Then this sensitivity function was applied to calibrate the observed spectrum of the scientific object (also see Lu et al. 2016b, 2019).

3.3 Correction of the Telluric Absorptions

In practice, we would better correct the telluric absorption at first, and then calibrate spectral fluxes. In this case, we do not need to mask the telluric absorption bands again during the spectral flux calibration. Following the method described in Section 2, we first use Equation (1) to model the observed spectra $\mathcal{S}(\lambda)$ of comparison star (in counts). Because the wavelength coverage of all observed spectra is about 5000 Å~9000 Å, these significant absorption bands listed in Table 1 are included, and they are masked in modelling process (see Fig. 3). Then we obtained the telluric transmission spectrum by dividing the observed spectrum $\mathcal{S}(\lambda)$ of the comparison star by the modelled spectrum $\mathcal{S}'(\lambda)$. In order to avoid introducing new errors

to the corrected spectrum of the scientific object, we set the transmission of the wavelength regions outside the telluric absorption windows to 1 before correcting the telluric absorption lines of the observed spectrum. This is reasonable because O_2 and H_2O molecular are fully transparent for the photons from these wavelength regions (see Smette et al. 2015). All transmission spectra (in the telluric absorption windows) calculated from above process were plotted annually in Figure 4, and we zoomed in the B3 absorption bands and over-plotted in Figure 4. The figure clearly shows that the telluric absorption depth presents significant variation. We first used the telluric transmission spectra to correct the telluric absorption lines of the observed spectra, then we obtained flux calibrated spectra using the steps described in Section 3.2. Figure 5 is an example for comparing the corrected spectra of telluric absorptions and uncorrected spectra, where the top panel is the spectra of the comparison star, and the bottom panel is the spectra of J1536.

3.4 Correction Accuracy of the Telluric Absorptions

As stressed in Section 3.1, we selected a special AGN of J1536 with redshift 0.3889 to put its [O III] $\lambda5007$ emission line drop into B2 telluric absorption bands, and developed a long-term spectroscopic monitoring, so that we can use the scatter of the [O III] $\lambda5007$ fluxes to estimate the correction accuracy of the telluric absorption lines. Strictly speaking, the [O III] $\lambda5007$ emission line of J1536 drops into the red side of B2 telluric absorption bands that dominated by H_2O molecular absorption.

In practice, the fluxes of forbidden line [O III] $\lambda5007$ emitted from the narrow-line region of active galactic nuclei is a constant over reverberation timescales ($\sim$ years), therefore it can be used as an internal flux calibration standard (e.g., Foltz et al. 1981; Peterson et al. 1982, 2002). Based on the reverberation mapping of active galactic nuclei undertaken by the Lijiang 2.4-meter telescope, Lu et al. (2016b) found that the [O III] $\lambda5007$ fluxes of NGC 5548 measured from flux calibrated spectra show a small fluctuation at a level of 2%, which is regarded as the accuracy of the flux calibration. Meanwhile, Lu et al. (2019) recently found that the [O III] $\lambda5007$ fluxes of Mrk 79 give rise to the apparent variation at a level of 5% over reverberation timescales. Lu et al. (2019) further found that, if the [O III] $\lambda5007$ emission region is an extended source, the varying observing conditions (e.g., varying seeing) would cause extra dispersion of the [O III] $\lambda5007$ fluxes. It should be noted that the [O III] $\lambda5007$ emission region of NGC 5548 approximates to the point source, and the [O III] $\lambda5007$ emission region of Mrk 79 is an extended source.

To directly understand the impacts of the telluric absorptions on the scientific spectra, we measured the
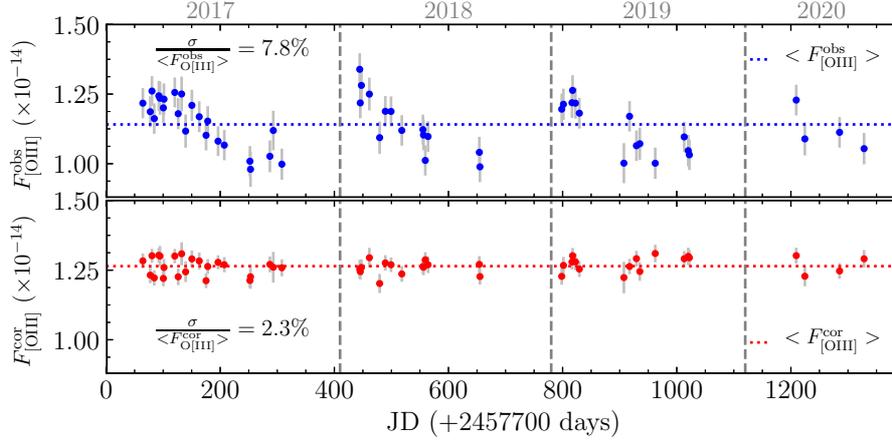
Fig. 6 The [O III] $\lambda5007$ fluxes of J1536 in units of erg s^{-1} cm^{-2}. The top panel shows the apparent variation of the [O III] $\lambda5007$ fluxes measured from the flux calibrated spectrum (before correcting the telluric absorption lines), periodicity is caused by the seasonal variability of the relative humidity. The bottom panel shows the scatter of the [O III] $\lambda5007$ fluxes measured from the flux calibrated and the telluric absorption corrected spectra. The year of observation was noted in the title of the panel.

Table 2 Statistics of the telluric absorption features. Col. (1) is the integral transparency of different absorption bands. Col. (2) is the absorber. The minimum, maximum and averaged value of the integral transparencies for the different absorption bands are listed in Cols. (3), (4) and (5), respectively. Col. (6) is the correlation analysis results (r, p) between the integral transparency and airmass. Col. (7) is the correlation analysis results (r, p) between the integral transparency and the width of star's flux distribution.

$\mathscr{T}_{B*}$ (1)	Molecular (2)	Min($\mathscr{T}_{B*}$) (3)	Max($\mathscr{T}_{B*}$) (4)	$\widehat{\mathscr{T}_{B*}}$ (5)	Airmass (6)	FWHM$_{star}$ (7)
$\mathscr{T}_{B1}$	O_2 (γ band)	0.985	0.996	0.991±0.003	(–0.25, 0.07)	(–0.07, 0.58)
$\mathscr{T}_{B2}$	O_2 (B band) + H_2O	0.934	0.976	0.961±0.011	(–0.52, 3.91×10^{-5})	(0.53, 1.85×10^{-5})
$\mathscr{T}_{B3}$	H_2O	0.846	0.979	0.926±0.039	(–0.41, 1.52×10^{-3})	(0.60, 8.36×10^{-7})
$\mathscr{T}_{B4}$	O_2 (A band)	0.811	0.863	0.847±0.011	(–0.90, 9.56×10^{-21})	(0.28, 0.03)
$\mathscr{T}_{B5}$	H_2O	0.917	0.996	0.964±0.024	(–0.43, 7.71×10^{-4})	(0.59, 1.22×10^{-6})

[O III] $\lambda5007$ fluxes of J1536 from the flux calibrated spectra. We used two continuum bands (4710−4740 Å and 5080−5110 Å in the rest frame) to set the continuum underneath the [O III] $\lambda5007$ and Hβ emission lines, then we integrated the continuum-subtracted [O III] $\lambda5007$ fluxes between 4980 Å and 5025 Å, and presented in the top panel of Figure 6. The figure shows the [O III] $\lambda5007$ fluxes before correcting the telluric absorption lines, demonstrating apparent period variation with a scatter of 7.8%. This scatter is larger than previous observation record (such as 5% of Mrk 79 and 2% of NGC 5548). The apparent period variation follows the seasonal variability of the relative humidity of Lijiang Observatory (see fig. 22 of Xin et al. 2020). Qualitatively, January is the deep winter of Lijiang Observatory, the atmospheric relative humidity is the lowest, then begins to increase slowly, and reaches the maximum in the rainy season (about from July to September). Therefore, accurate calibration of the telluric absorption lines from the observed spectrum is crucial for obtaining credible scientific data.

As a comparison, we also measured the [O III] $\lambda5007$ fluxes of J1536 from the flux calibrated and the telluric absorption corrected spectra. The measurement results were plotted in the bottom panel of Figure 6 for comparing with the measurements before correcting the telluric absorption lines, which shows that the scatter of the [O III] $\lambda5007$ fluxes is 2.3%, and the apparent period variation presented in the top panel is disappeared. As addressed above, the fluxes of [O III] $\lambda5007$ are stable enough in the timescale of years if the [O III] $\lambda5007$ emission region is compact. In practice, the scatter of [O III] $\lambda5007$ fluxes (2.3%) is caused by the accuracy of flux calibration and the accuracy of the telluric absorption correction. If we assume that the flux calibration accuracy of J1536 is the same with our previous experiment of NGC 5548 (i.e., 2%, Lu et al. 2016b), this means that the correction accuracy of the telluric absorption lines using the method described in Section 2 is 1%. In addition, in order to intuitively inspect the differences before and after correcting the telluric absorptions, we plotted the telluric
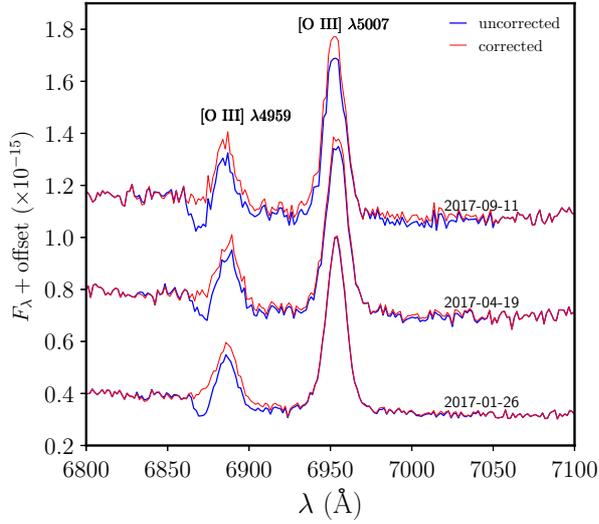
Fig. 7 The telluric absorption corrected and uncorrected [O III] profiles from the observation of 2017 (in the observed frame), observation dates are noted, the units of F_λ are erg s^{-1} cm^{-2} Å^{-1}. The differences of [O III] profiles before and after correcting the telluric absorptions are presented clearly.

absorption corrected and uncorrected [O III] profiles selected randomly from observations of 2017 in Figure 7. The figure also demonstrates the differences of the telluric absorption from the different observations.

3.5 Telluric Absorption Features of Lijiang Observatory

In order to understand the variation of the telluric absorptions caused by the molecular of O_2 and H_2O or both together at Lijiang Observatory, we calculated the integral transparency (denoted by $\mathscr{T}_{B*}$) of each absorption band using formula of $\int_{\lambda1}^{\lambda2} \mathcal{T}(\lambda)\, d\lambda/(\lambda2 - \lambda1)$ (where $\lambda1$ and $\lambda2$ are the edges of the telluric absorption bands, $\mathcal{T}(\lambda)$ is the telluric transmission spectrum), and plotted them as the functions of time in Figure 8, where "B∗" means the number of the telluric absorption band, which corresponds to the number of Table 1. Inspecting the figure, we can see that the variation of the integral transparency for the telluric absorption bands mainly or fully caused by the molecular of H_2O (i.e., B2, B3 and B5 absorption bands) is similar with the apparent period variation of the [O III] $\lambda5007$ fluxes that contaminated by the H_2O absorption (the top panel of Fig. 6). The seasonal variability of the H_2O absorption bands is clearly visible, which is consistent with the seasonal variability of the relative humidity (see also fig. 22 of Xin et al. 2020). Meanwhile, the integral transparency for the absorption bands caused by the molecular of O_2 (i.e., B1 and B4 absorption bands) do not present obvious variation trend in the time domain. In the varing observing conditions,

the averaged integral transparency ($\widehat{\mathscr{T}_{B1}}$, $\widehat{\mathscr{T}_{B2}}$, $\widehat{\mathscr{T}_{B3}}$, $\widehat{\mathscr{T}_{B4}}$ and $\widehat{\mathscr{T}_{B5}}$) of the telluric absorption bands (B1, B2, B3, B4 and B5) is (0.991, 0.961, 0.926, 0.847 and 0.964) with scatter (i.e., standard deviation) of (0.3%, 1.1%, 3.9%, 1.1% and 2.4%), this means that about (1%, 4%, 7%, 15% and 4%) of photons propagated from the distant objects are absorbed by the O_2 or H_2O in these absorption windows, respectively. We also listed the minimum and maximum of the integral transparencies in Table 2.

We calculated the airmass in the middle of the exposure time, and investigated the relation between the integral transparency and airmass. The integral transparency as a function of airmass was presented in Figure 9. We calculated the Spearman correlation coefficient between the integral transparency and airmass and listed in Table 2. These analyses show that the integral transparency of the O_2 absorption band is well correlated with airmass, and the integral transparency of the H_2O absorption bands can also be effected by airmass. In addition, we measured the width (FWHM$_{star}$) of star's flux distribution from the short exposure image observed before and near the spectroscopy, and showed the relation between the integral transparency and the FWHM$_{star}$ in Figure 10. We also calculated the Spearman correlation coefficient between the integral transparency and the FWHM$_{star}$ and listed in Table 2. In practice, the variation of FWHM$_{star}$ is mainly modulated by varying seeing, where seeing is always changing. These analyses show that the integral transparency of the H_2O absorption bands correlates with the variation of FWHM$_{star}$.

4 DISCUSSION

In the ground-based optical spectrum, the telluric absorption bands are caused by two kinds of absorbers: molecular oxygen (O_2) and water vapour (H_2O). Based on the long slit spectroscopy, we provide a accurate correction method for the telluric absorption lines using the observed comparison star spectrum and stellar spectral library, the correction accuracy is 1%. Our correction method for the telluric absorption lines has many advantages over the traditional method (i.e., observing the telluric standard star), especially in the study of long-term spectral monitoring. For example, (1) the scientific object and its comparison star are observed simultaneously in the long slit with the same observing conditions, such as the same airmass and seeing. Therefore, it is possible that the correction accuracy of the telluric absorption lines using this method (1%) should be better than the traditional method; (2) in the long-term spectral monitoring project, we do not need to take expensive telescope time to observe the telluric standard star in each sampling. Therefore, in the research of one-epoch spectral observation or long-term spectroscopic monitoring, this work provides a kind
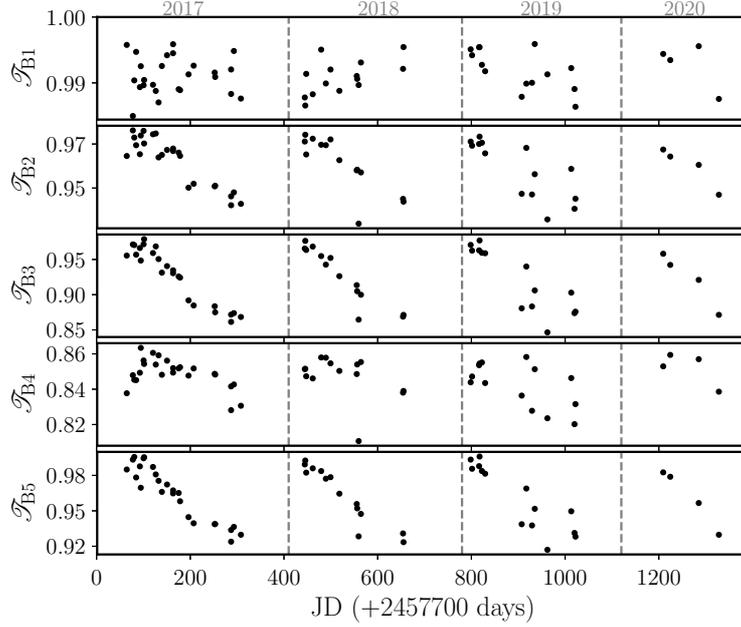
Fig. 8 The integral transparency ($\mathscr{T}_{B1}$, $\mathscr{T}_{B2}$, $\mathscr{T}_{B3}$, $\mathscr{T}_{B4}$ and $\mathscr{T}_{B5}$) of the telluric absorption band (B1, B2, B3, B4 and B5, see Table 1) as a function of time, respectively. The observation started from 2017 and continued to 2020, and the annual spectral sampling almost lasts from January to September. The year of observation was noted in the title of the panel.
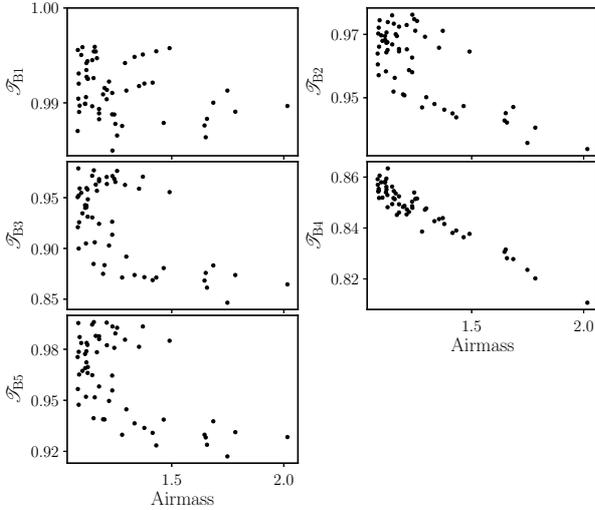
Fig. 9 Relationship between the integral transparency and airmass. The results of correlation analysis are listed in Table 2.

Fig. 10 Relationship between the integral transparency and the width of star's flux distribution ($\mathrm{FWHM_{star}}$, measured from the short exposure image observed before and near the spectroscopy). The results of correlation analysis are listed in Table 2.

of worthy observation strategy and corresponding method to correct the telluric absorptions.

As described in Section 2, the telluric transmission spectrum is obtained from the process of fitting the observed spectrum of comparison star by stellar template through masking the discrete absorption windows. The discrete absorption windows mean we can select the continuum windows in the spectral fitting process. In this work, we only apply this method described in Section 2 to the spectrum that its wavelength covers less

than 9000 Å, which is limited by the spectrograph of YFOSC. Actually, because the wavelength ranges from 9000 Å to around 17000 Å exist the available continuum windows (see the synthetic telluric absorption spectrum calculated by Smette et al. (2015) using the Line by Line Radiative Transfer Model, the telluric absorption bands are also discrete), the application of this method can be extrapolated from optical the region to 17000 Å.

The telluric transparency of the B4 absorption band caused by oxygen has the largest value, and has the strongest correlation with airmass but it has no correlation with the seeing. Meanwhile, the telluric transparency of the B1 absorption band also caused by oxygen has the smallest value, which does not correlate with airmass and seeing (see Sect. 3.5). However, not only the airmass but also seeing correlates with the telluric transparency of water vapour absorption (e.g., B3 and B5 bands). These results show that (1) the absorptions of oxygen and water vapour in the optical spectrum closely correlate with atmospheric depth, and (2) the oxygen concentration of the observation site does not change with the varying seeing while the amount of water changes with the varying seeing. In addition, analysis results of Section 3.5 show that the red side of the optical spectrum including emission lines and continuum would be affected by the varying telluric absorptions and accurate correction of the telluric absorption lines should benefit from spectral flux calibration.

5 SUMMARY

In this paper, combining the advantages of long slit spectroscopy, we described a method that can be used to accurately correct the telluric absorption lines of spectrum. We constructed the telluric transmission spectrum by fitting the observed spectrum of the comparison star by the stellar template, then obtained the telluric absorption corrected spectrum by dividing the observed spectrum by the telluric transmission spectrum. We applied this method to correct the telluric absorption lines of the long-term monitored spectra by the Lijiang 2.4-meter telescope. Using the scatter of the [O III] $\lambda5007$ fluxes emitted from the narrow-line region of active galactic nuclei (SDSS J153636.22+044127.0) as an indicator, we found that the correction accuracy of this method for the telluric absorption lines is 1%. We investigated the telluric absorption features of Lijiang Observatory, and found that the telluric absorption transparency correlates with the relative humidity, airmass and seeing. This work provides a kind of worthy observation strategy and corresponding method to correct the telluric absorptions.

References

Bertaux, J. L., Lallement, R., Ferron, S., Boonne, C., & Bodichon, R. 2014, A&A, 564, A46

Boroson, T. A., & Lauer, T. R. 2009, Nature, 458, 53

Cotton, D. V., Bailey, J., & Kedziora-Chudczer, L. 2014, MNRAS, 439, 387

Du, P., Lu, K.-X., Hu, C., et al. 2016, ApJ, 820, 27

Fan, Y.-F., Bai, J.-M., Zhang, J.-J., et al. 2015, RAA (Research in Astronomy and Astrophysics), 15, 918

Foltz, C. B., Peterson, B. M., Cariotti, E. R., et al. 1981, ApJ, 250, 508

Gullikson, K., Dodson-Robinson, S., & Kraus, A. 2014, AJ, 148, 53

Hanson, M. M., Conti, P. S., & Rieke, M. J. 1996, ApJS, 107, 281

Hanson, M. M., Kudritzki, R. P., Kenworthy, M. A., Puls, J., & Tokunaga, A. T. 2005, ApJS, 161, 154

Husser, T. O., Wende-von Berg, S., Dreizler, S., et al. 2013, A&A, 553, A6

Kaspi, S., Smith, P. S., Netzer, H., et al. 2000, ApJ, 533, 631

Lu, K.-X., Li, Y.-R., Bi, S.-L., & Wang, J.-M. 2016a, MNRAS, 459, L124

Lu, K.-X., Du, P., Hu, C., et al. 2016b, ApJ, 827, 118

Lu, K.-X., Bai, J.-M., Zhang, Z.-X., et al. 2019, ApJ, 887, 135

Lucy, L. B. 1974, AJ, 79, 745

Maiolino, R., Rieke, G. H., & Rieke, M. J. 1996, AJ, 111, 537

Maoz, D., Netzer, H., Leibowitz, E., et al. 1990, ApJ, 351, 75

Peterson, B. M., Foltz, C. B., Byard, P. L., & Wagner, R. M. 1982, ApJS, 49, 469

Peterson, B. M., Berlind, P., Bertram, R., et al. 2002, ApJ, 581, 197

Richardson, W. H. 1972, Journal of the Optical Society of America (1917-1983), 62, 55

Seifahrt, A., Käufl, H. U., Zängl, G., et al. 2010, A&A, 524, A11

Smette, A., Sana, H., Noll, S., et al. 2015, A&A, 576, A77

Vacca, W. D., Cushing, M. C., & Rayner, J. T. 2003, PASP, 115, 389

Wang, C.-J., Bai, J.-M., Fan, Y.-F., et al. 2019, RAA (Research in Astronomy and Astrophysics), 19, 149

Xin, Y.-X., Bai, J.-M., Lun, B.-L., et al. 2020, RAA (Research in Astronomy and Astrophysics), 20, 149

Zhang, S., Zhou, H., Shi, X., et al. 2019, ApJ, 877, 33